Starlink-26 satellite re-entry determination

A.I. Nazarenko. April 2021
anazarenko32@mail.ru, satmotion.ru

1. IADC 2021 test campaign

The current test object is the starlink-26 satellite (identified via cospar id 2019-029f or norad id 44240). it was launched from Kennedy space center (etr, united states) on 2019-05-24 02:24utc into an orbit with an approximate perigee height of 442 km and an approximate apogee height of 445 km, with an inclination of 53 deg. the satellite has a flat box shape of dimensions 3.7m length, 1.5m width and 0.2m height, with 1 solar panel deployed which could be perpendicular or parallel to the satellite body, with 2.8m length and 8.1m width, with a dry mass of about 227 kg.

Its orbit on 22-march-2021 had approximately a perigee and apogee height of 317 km and 320 km with a 53 deg inclination. with this, and depending on the atmospheric model used, a re-entry between 2 and 11 April 2021 is expected.

2. Technique of re-entry determination

To solve the problem in question, the author used the methodology of the optimal filtration of measurements, which is detailed in the articles [1], [2] and book [3]…As a result of analysis, the comparative relationships were established between the errors of state vector estimates with using the considered methods (approaches). The analysis results are presented. It is seen from this data that, for any level of disturbances, *thebest accuracy is achieved with applying the optimal measurement filtering technique*.The expediency of LST application *without* or *with* state vectorextension depends on the level of disturbances. There existssome level of small disturbances, at which it is more expedient toapply LST without state vector extension. However, even in thiscase the errors are greater, than in the case of using the optimalfiltration of measurements (the nonparametric approach).

3. Results. April 05 The

As the initial data, the TLE from site of Combined Space Operations Center (CSpOC) [3] are used (see Table 1).

Table 1. Initial TLE values

1 44240U 19029F   21086.57536359 +.00658016 +17910-3 +22060-2 0 09994
2 44240 052.9912 233.1619 0010488 317.3866 042.6344 15.89484802103022
1 44240U 19029F   21086.70110831 +.00684801 +19443-3 +22751-2 0 09993
2 44240 052.9915 232.5214 0010687 317.9347 042.0856 15.89659893103048
1 44240U 19029F   21087.39245847 +.00634550 +16883-3 +20108-2 0 09990
2 44240 052.9915 228.9956 0011245 322.1213 037.9020 15.90577205103933

```
1 44240U 19029F   21087.51811190 +.00795589 +26820-3 +24883-2 0 09990
2 44240 052.9909 228.3554 0011376 323.0255 036.9984 15.90835013103173
1 44240U 19029F   21087.70656876 +.00732354 +22679-3 +22620-2 0 09995
2 44240 052.9904 227.3925 0011445 323.8498 036.1752 15.91073170103986
1 44240U 19029F   21088.71122468 .00643739 17732-3 18710-2 0  9999
2 44240 52.9893 222.2555 0012084 327.8085 32.2201 15.92230120103361
1 44240U 19029F   21088.71122468 .00643739 17732-3 18710-2 0  9999
2 44240 52.9893 222.2555 0012084 327.8085 32.2201 15.92230120104148
1 44240U 19029F   21089.08778468 .00573158 14175-3 16308-2 0  9993
2 44240 52.9892 220.3284 0012418 329.6681 30.3625 15.92631610104203
1 44240U 19029F   21089.52696459 .00632160 17313-3 17446-2 0  9991
2 44240 52.9891 218.0785 0012648 331.7267 28.3071 15.93203176104273
1 44240U 19029F   21089.65241761 .00600187 15650-3 16441-2 0  9997
2 44240 52.9896 217.4362 0012753 332.0488 27.9851 15.93342156103517
1 44240U 19029F   21089.65241761 .00600187 15650-3 16441-2 0  9997
2 44240 52.9896 217.4362 0012753 332.0488 27.9851 15.93342156104293
1 44240U 19029F   21089.65241769 .00637467 17638-3 17449-2 0  9993
2 44240 52.9896 217.4362 0012760 332.1903 27.8439 15.93355220104291
1 44240U 19029F   21090.34219195 .00613150 16500-3 16050-2 0  9996
2 44240 52.9893 213.8991 0013137 335.0419 24.9970 15.94186127103622
1 44240U 19029F   21090.71826153 .00736902 24110-3 18690-2 0  9994
2 44240 52.9892 211.9703 0013352 336.8007 23.2415 15.94771129104463
1 44240U 19029F   21091.21945717 .00870280 34590-3 21053-2 0  9996
2 44240 52.9882 209.3962 0013360 337.9293 22.1157 15.95658818103761
1 44240U 19029F   21091.21945717 .00870280 34590-3 21053-2 0  9996
2 44240 52.9882 209.3962 0013360 337.9293 22.1157 15.95658818104548
1 44240U 19029F   21091.53254863 .01068272 54577-3 24943-2 0  9995
2 44240 52.9877 207.7856 0013358 338.3314 21.7147 15.96346882104597
1 44240U 19029F   21091.84551697 .00964886 44029-3 21769-2 0  9993
2 44240 52.9863 206.1724 0013322 339.7088 20.3408 15.96948676103866
1 44240U 19029F   21091.84551697 .00964886 44029-3 21769-2 0  9993
2 44240 52.9863 206.1724 0013322 339.7088 20.3408 15.96948676104643
1 44240U 19029F   21091.90809634 .00971684 44805-3 21769-2 0  9993
2 44240 52.9882 205.8497 0012734 335.6989 24.3778 15.97092220104659
1 44240U 19029F   21092.53358959 .01112864 61823-3 23158-2 0  9993
2 44240 52.9908 202.6207 0012529 339.7636 20.2858 15.98456501104750
1 44240U 19029F   21092.59611014 .01053007 54685-3 21774-2 0  9996
2 44240 52.9849 202.2991 0013693 341.8068 18.1959 15.98522105104769
1 44240U 19029F   21092.78366116 .01011345 50284-3 20483-2 0  9993
2 44240 52.9837 201.3330 0013833 342.4855 17.5694 15.98875739104785
1 44240U 19029F   21092.78366116 .01091706 59675-3 22077-2 0  9996
2 44240 52.9863 201.3247 0013280 338.0476 22.0448 15.98938493104793
```

1 44240U 19029F   21093.15857712 .01137880 66431-3 21981-2 0 9990
2 44240 52.9861 199.3894 0012546 337.4648 22.5706 15.99776745104853
1 44240U 19029F   21093.42998043 .00879608 37798-3 16634-2 0 9996
2 44240 52.9835 197.9885 0012510 344.8443 139.1129 16.00087157104897
1 44240U 19029F   21093.47094370 .01105800 62838-3 20691-2 0 9999
2 44240 52.9835 197.7764 0012511 345.4631 14.6486 16.00324543104906
1 44240U 19029F   21093.53338277 .01097756 61926-3 20408-2 0 9996
2 44240 52.9870 197.4579 0012503 344.8956 15.1238 16.00435009104912
1 44240U 19029F   21093.84557786 .01058408 57589-3 18966-2 0 9995
2 44240 52.9819 195.8316 0014533 345.3301 14.7247 16.01002287104960
1 44240U 19029F   21094.15762666 .00942788 44913-3 16422-2 0 9999
2 44240 52.9796 194.2174 0014250 347.9432 11.8537 16.01467862105019
1 44240U 19029F   21094.48384264 .01081254 61564-3 18195-2 0 9992
2 44240 52.9828 192.5192 0013526 348.2463 93.7748 16.02111446105062
1 44240U 19029F   21094.84383545 .01024740 55245-3 16520-2 0 9999
2 44240 52.9843 190.6503 0013119 348.3694 11.6645 16.02831323105124

The results of the optimal measurement filtration technique to determine the current drag parameter (ballistic factor) are presented in Figure 1.

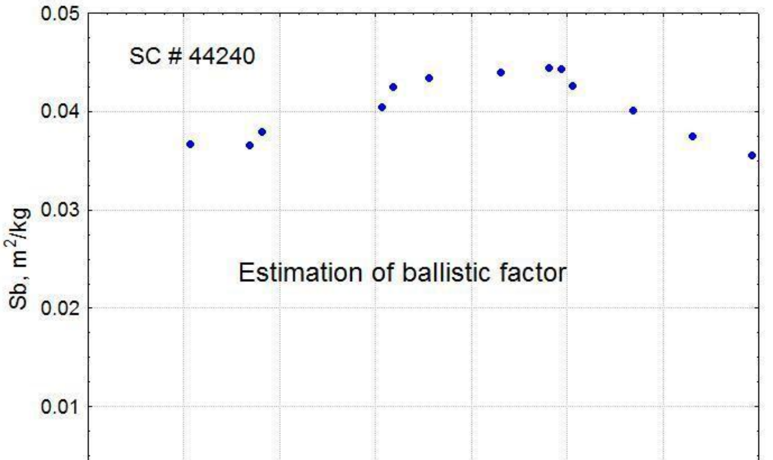

Figure 1. Estimation of ballistic factor (Sb)

Here, the deviations of the current ratings of the Sb from the average value do not exceed ±11%. Table 2 provides estimates of the time of entry into the dense atmosphere (reaching an altitude of 80 km).

.Таблица 2. Determination of reentry time

Time from April 01		Date	hh	mm
Initial	Reentry			
0.219	9.456	April 10	10	56
3.47	8.641	April 09	15	22

Here, the differences in entry time estimates correspond to variations of Sb values.

6. Results. April 06

The results of the optimal measurement filtration technique to determine the current drag parameter (ballistic factor) are presented in Figure 2.

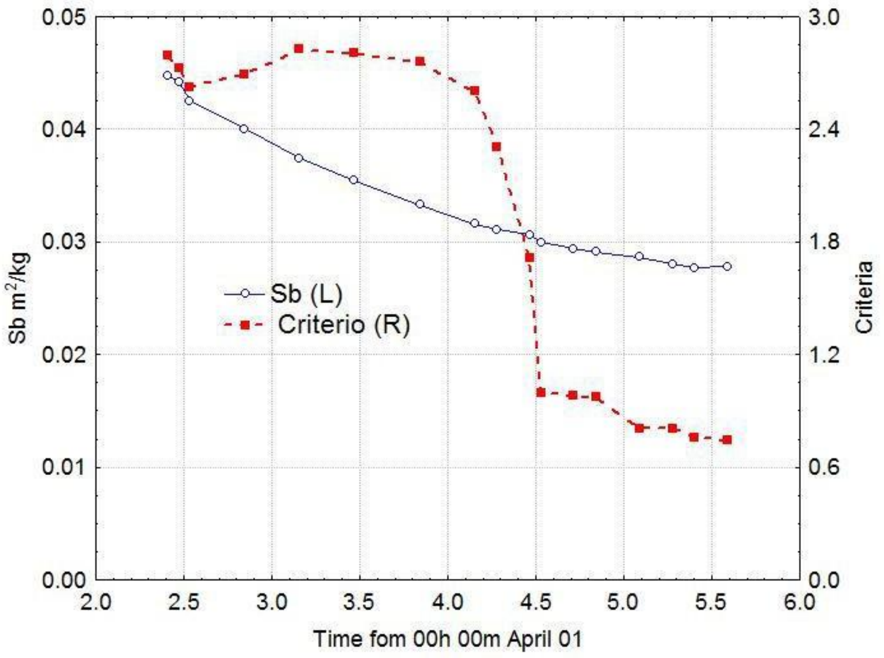

Figure 2. Estimation of ballistic factor (Sb) and minimizing criteria

These data show that ballistic coefficient estimates are stabilizing. The proximity of the minimizable criteria to 1 indicates that the constructed orbit fits well into the measurements.Table 3 provides all estimates of the time of entry into the dense atmosphere (reaching an altitude of 80 km).

Таблица 3. Determination of reentry time

Time from April 01		Date	hh	mm
Initial	Reentry			
0.219	9.456	April 10	10	56
3.47	8.641	April 09	15	22
4.841	9.750	April 10	17	59
5.090	8.820	April 10	19	41
5.401	9.941	April 10	22	35
5.588	9.883	April 10	**21**	**11**

The data of the last two lines show the stabilization of estimates of the re-entry time. This is a consequence of the stabilization of Sb's estimates.

Figure 3 shows the Earth map and a calculated route of the satellite's movement at re-entry. The red color highlights the possible scattering of the entry point into the dense layers of the atmosphere.

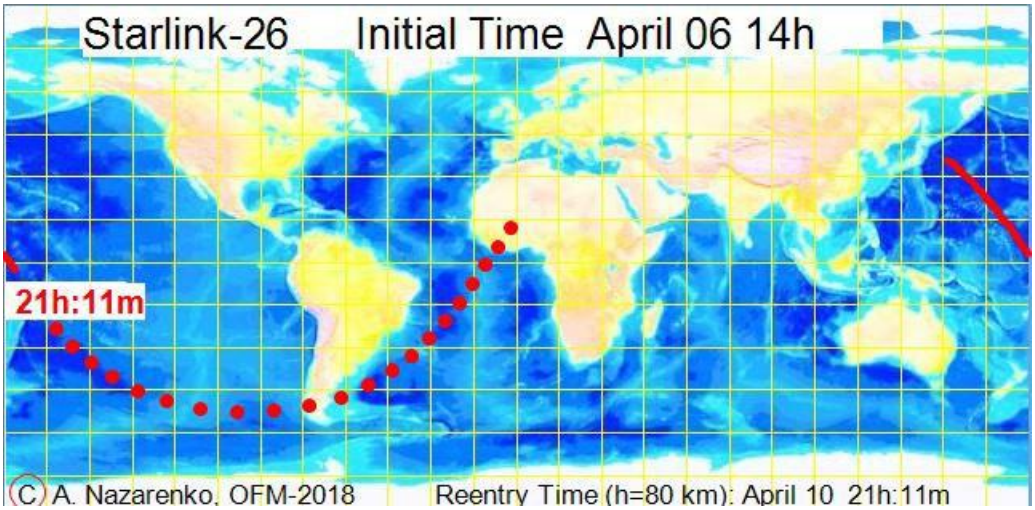

Figure 3. Calculated re-entry route

7. Results. April 07

The results of the optimal measurement filtration technique to determine the current drag parameter (ballistic factor) are presented in Figure 4.

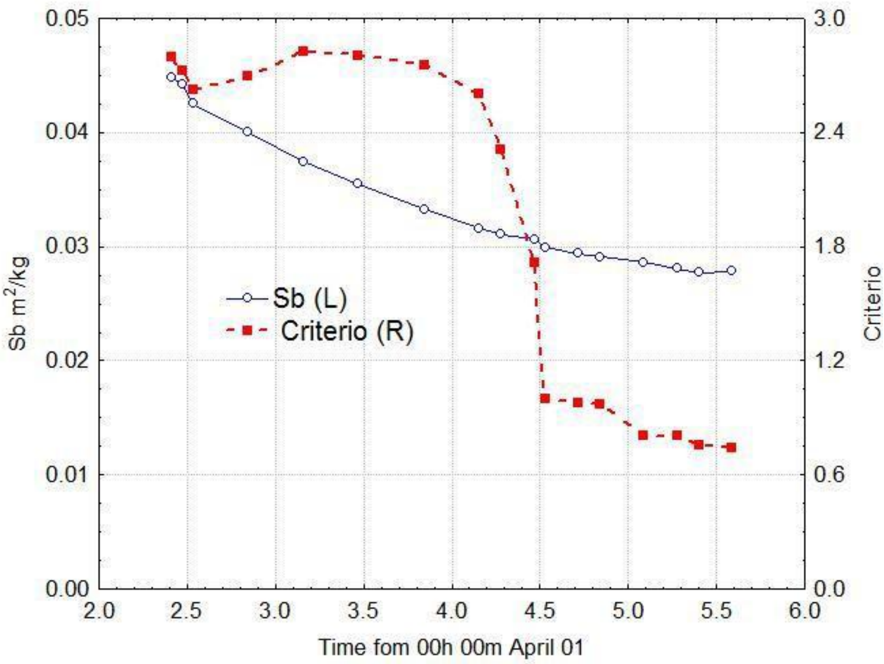

Figure 4. Estimation of ballistic factor (Sb) and minimizing criterio

These data show that ballistic coefficient estimates are stabilizing. The proximity of the minimizable criteria to 1 indicates that the constructed orbit fits well into the measurements. Table 4 provides all estimates of the time of entry into the dense atmosphere (reaching an altitude of 80 km).

Таблица 4. Determination of **re-entry time**

Time from April 01		Date	hh	mm
Initial	Reentry			
0.219	9.456	April 10	10	56
3.47	8.641	April 09	15	22

4.841	9.750	April 10	17	59
5.090	8.820	April 10	19	41
5.401	9.941	April 10	22	35
5.588	9.883	April 10	21	11
5.712	9.799	April 10	19	09
6.209	9.736	April 10	17	39

The data of the last two lines show the the approach of the re-entry time by 1.5 hours (2% of the life time). This is the result of a small increase in the Sb value.

Figure 5 shows the Earth map and the calculated route of the satellite's movement at re-entry. The red color highlights the possible scattering of the entry point into the dense layers of the atmosphere.

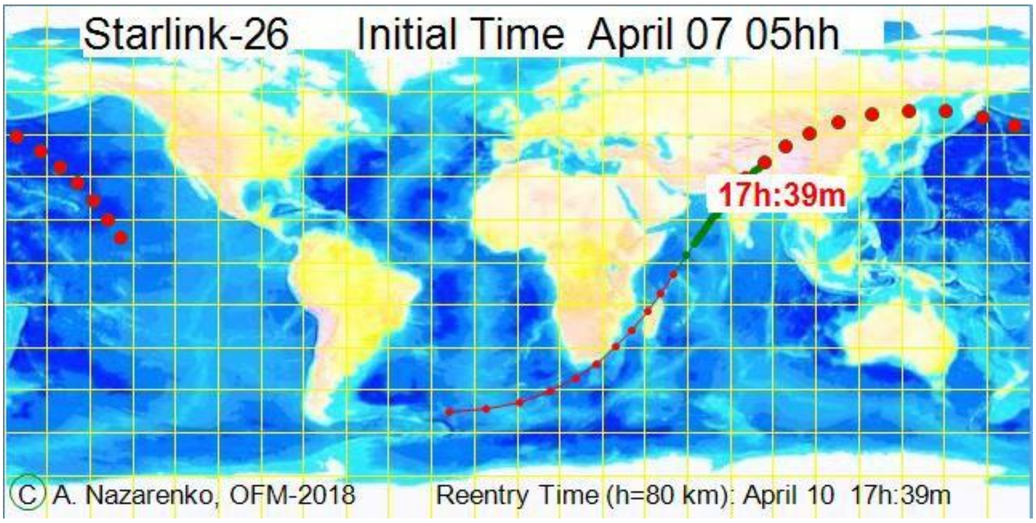

Figure 5. Calculated re-entry route

8. Results. April 08

The results of the optimal measurement filtration technique to determine the current drag parameter (ballistic factor) are presented in Figure 6.

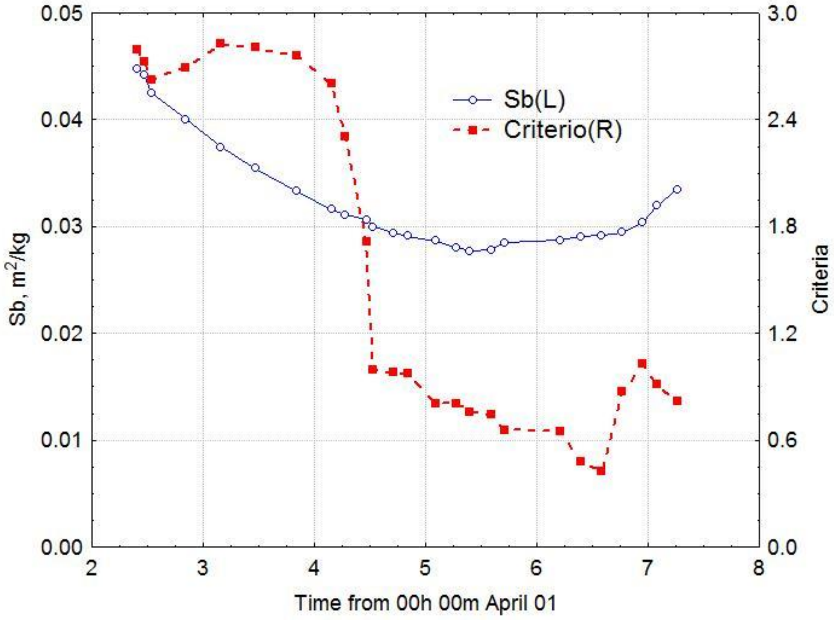

Figure 6. Estimation of ballistic factor (Sb) and minimizing criteria

From these data you can see the growth of the satellite's drag over the last 24 hours. Sb's valuea increased by 22%. This is a very significant increase. That is due to the impact of a geomagnetic storm that occurred on 7 April (see figure 7)

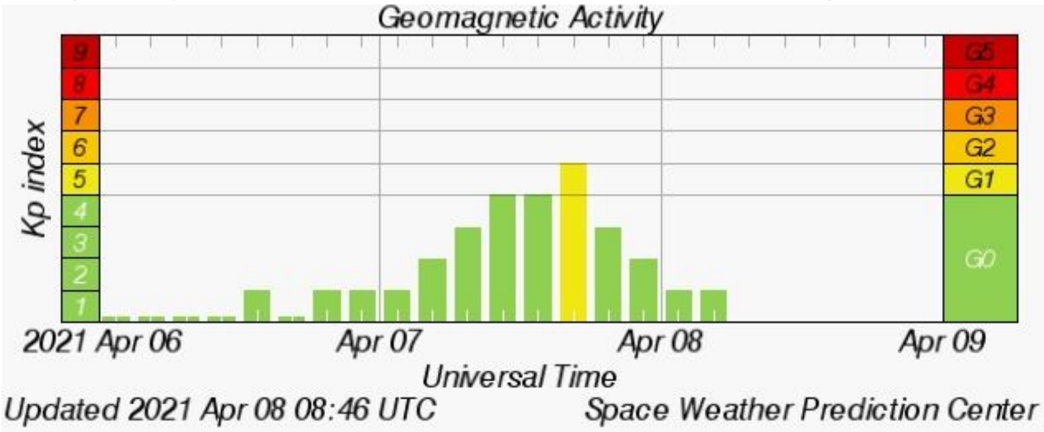

Figure 7. Geomanite activity. Kp index values

In the previous forecast of the re-entry time, the impact of a possible geomagnetic storm was not taken into account. Therefore, it should be expected that the increase in the Sb value will lead to a significant diminution of the estimated re-entry time (≈ 20% of the life time).

Table 4 provides all estimates of the time of entry into the dense atmosphere (reaching an altitude of 80 km).

Таблица 4. Determination of **re-entry time**

Time from April 01		Date	hh	Mm
Initial	Reentry			
0.219	9.456	April 10	10	56
3.47	8.641	April 09	15	22
4.841	9.750	April 10	17	59
5.090	8.820	April 10	19	41
5.401	9.941	April 10	22	35
5.588	9.883	April 10	21	11
5.712	9.799	April 10	19	09
6.209	9.736	April 10	**17**	**39**
7.264	9.062	April 10	**01**	**29**

The data of the last two lines show the the diminution of the re-entry time by 16 hours (21% of the life time). This is the result of increase in the Sb value.

Figure 8 shows the Earth map and the calculated route of the satellite's movement at re-entry. The red color highlights the possible scattering of the entry point into the dense layers of the atmosphere.

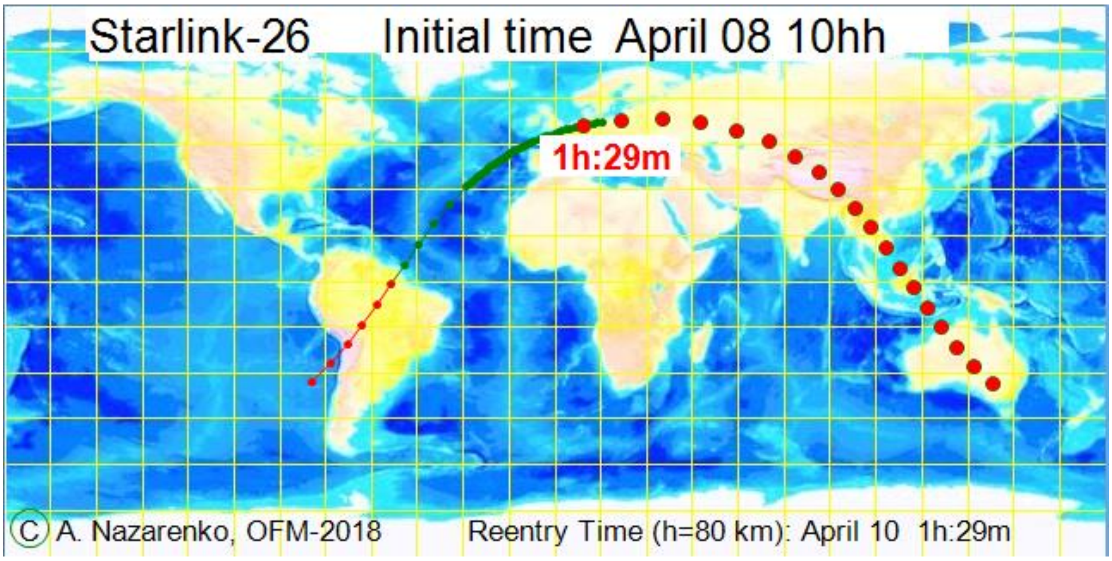

Figure 8. Calculated re-entry route

From these data it is clear that the combustion of the satellite during re-entry can be observed from the territory of Russia.

9. Results. April 09 morning

The results of the optimal measurement filtration technique to determine the current drag parameter (ballistic factor) are presented in Figure 9.

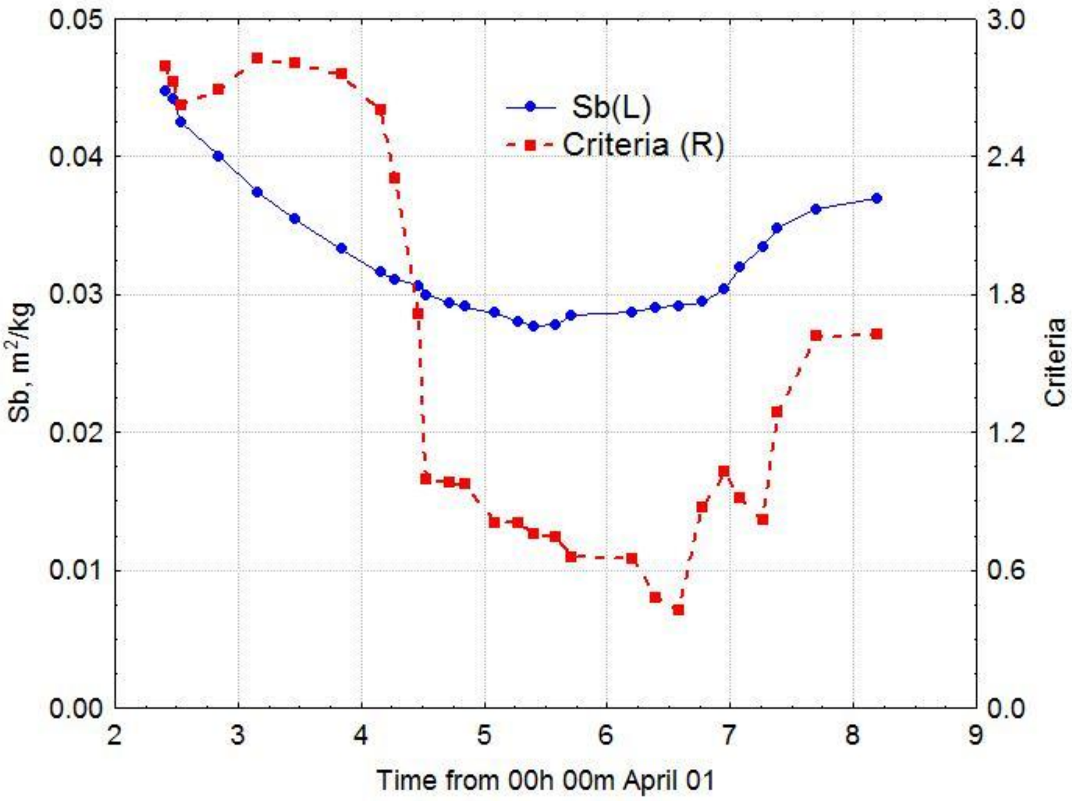

Figure 9. Estimation of ballistic factor (Sb) and minimizing criteria

It is clear from these data that the Sb estimates have stabilized.

Table 5 provides all estimates of the time of entry into the dense atmosphere (reaching an altitude of 80 km).

Таблица 5. Determination of **re-entry time**

Time from April 01		Date	hh	mm
Initial	Reentry			
0.219	9.456	April 10	10	56
3.47	8.641	April 09	15	22
4.841	9.750	April 10	17	59
5.090	8.820	April 10	19	41
5.401	9.941	April 10	22	35
5.588	9.883	April 10	21	11
5.712	9.799	April 10	19	09
6.209	9.736	April 10	**17**	**39**
7.264	9.062	April 10	**01**	**29**
7.388	9.024	April 10	**00**	**35**
7.697	9.045	April 10	**01**	**05**
8.191	9.188	April 10	**04**	**31**

The data of the last two lines show the increase of the re-entry time by 3 hours 26 minutes (15% of the life time). This is the result of weakening of drag in the atmosphere after the geomagnetic storm.

Figure 10 shows the Earth map and the calculated route of the satellite's movement at re-entry. The red color highlights the possible scattering of the entry point into the dense layers of the atmosphere.

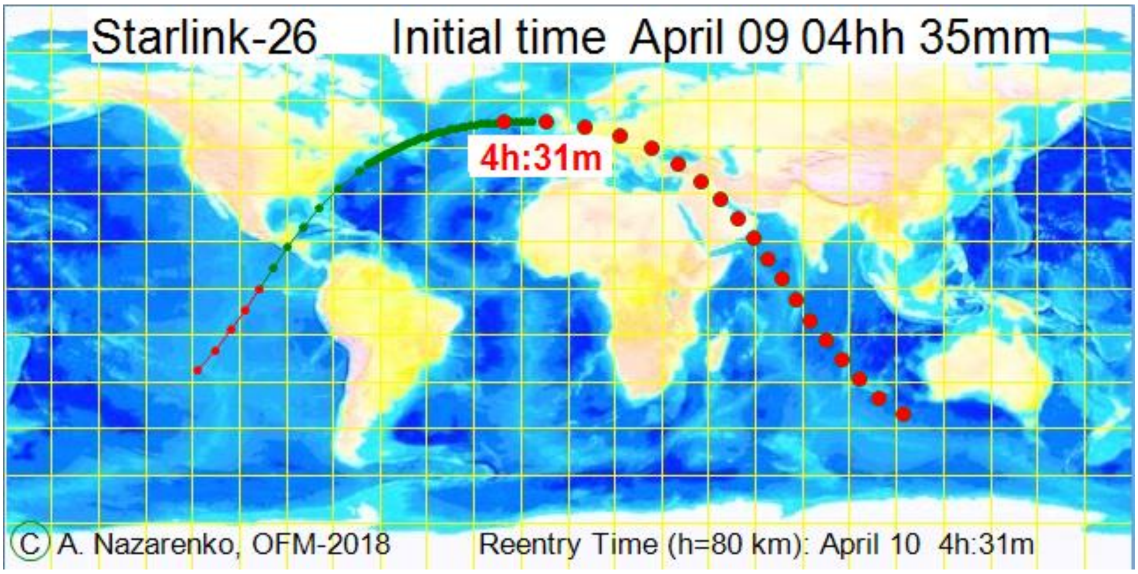

Figure 10. Calculated re-entry route

From these data it is clear that the combustion of the satellite during re-entry can be observed from the territory of Europe and Russia.

10. Results. April 09 evening

The results of the optimal measurement filtration technique to determine the current drag parameter (ballistic factor) are presented in Figure 11.

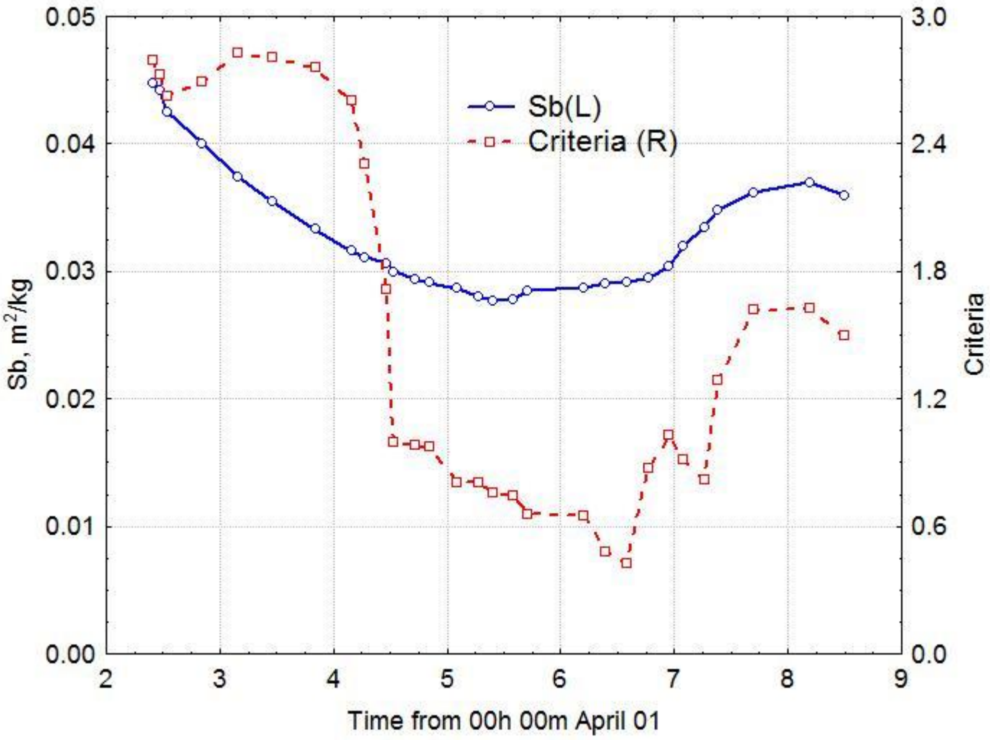

Figure 11. Estimation of ballistic factor (Sb) and minimizing criteria

It is clear from these data that the Sb estimates began to diminish. They decreased by 3%. This is to be expected, as the geomagnetic storm ended on the night of April 7.

Table 6 provides all estimates of the time of entry into the dense atmosphere (reaching an altitude of 80 km).

Таблица 5. Determination of **re-entry time**

Time from April 01		Date	hh	mm
Initial	Reentry			
0.219	9.456	April 10	10	56
3.47	8.641	April 09	15	22
4.841	9.750	April 10	17	59
5.090	8.820	April 10	19	41
5.401	9.941	April 10	22	35
5.588	9.883	April 10	21	11
5.712	9.799	April 10	19	09
6.209	9.736	April 10	**17**	**39**
7.264	9.062	April 10	**01**	**29**
7.388	9.024	April 10	**00**	**35**
7.697	9.045	April 10	**01**	**05**
8.191	9.188	April 10	04	31
8.499	9.260	April 10	**06**	**14**

The data of the last two lines show the increase of the re-entry time by 1 hour 43 minutes (9% of the life time). This is the result of weakening of drag in the atmosphere after the geomagnetic storm.

Figure 12 shows the Earth map and the calculated route of the satellite's movement at re-entry. The red color highlights the possible scattering of the entry point into the dense layers of the atmosphere.

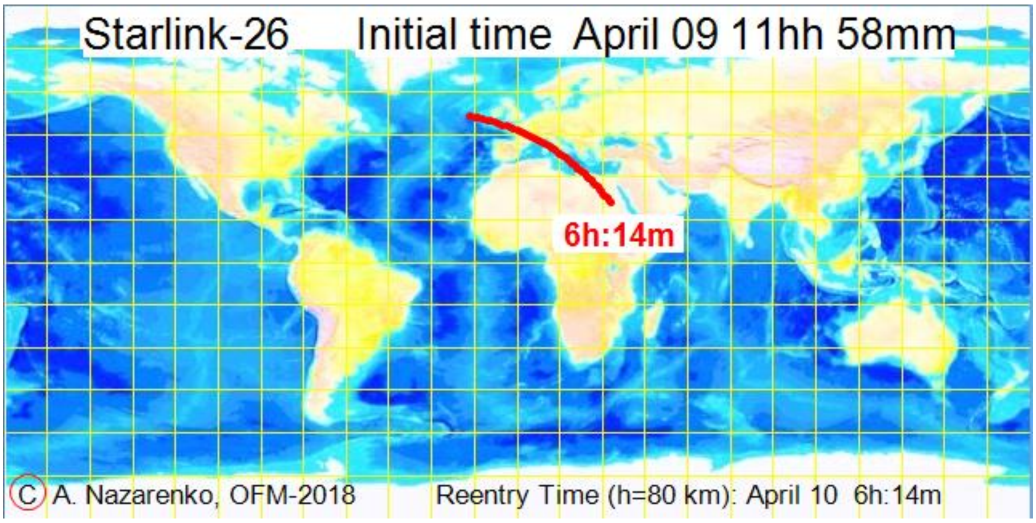

Figure 12. Calculated re-entry route

11.Results. April 10. Totals

This section was prepared after the satellite re-entry. It provides the latest results. The last set of TLE was added, relating to the time of 21099.62231585 (April 09, 14h 56m). The fit span consisting of 11 sets of TLE has been applied. They are shown below in Table 6.

Table 6. Latest TLE

```
1 44240U 19029F   21097.39564267  .01776694  24259-2  19549-2 0  9990
2 44240  52.9845 177.3445 0013700   0.1849 359.9186 16.09406088105529
1 44240U 19029F   21097.58188674  .02012914  35466-2  21426-2 0  9993
2 44240  52.9849 176.3709 0013230   3.1902 356.9115 16.10206609105557
1 44240U 19029F   21097.76802460  .02428941  69045-2  25503-2 0  9990
2 44240  52.9804 175.3938 0013408   2.9085 357.2024 16.11233106104811
1 44240U 19029F   21097.95404333  .02574049  93650-2  26185-2 0  9995
2 44240  52.9804 174.4141 0012916   2.3489 357.7793 16.12331862105618
1 44240U 19029F   21098.07798162  .02586888  10054-1  25362-2 0  9991
2 44240  52.9792 173.7617 0013023   3.0668 357.0444 16.13052656105631
1 44240U 19029F   21098.27541653  .02636556  12420-1  24929-2 0  9999
2 44240  52.9787 172.7159 0010730 356.9199  70.8329 16.14255819105679
1 44240U 19029F   21098.38759118  .02592036  11737-1  23115-2 0  9998
2 44240  52.9789 172.1292 0012640   3.2998 356.8118 16.14886992105691
1 44240U 19029F   21098.69682150  .02234647  63818-2  16177-2 0  9992
2 44240  52.9794 170.4974 0013939   4.7848 355.0219 16.16497329105740
1 44240U 19029F   21099.19106138  .03886443  11865-4  19594-2 0  9996
2 44240  52.9832 167.8679 0013564   1.2920 359.0854 16.19733203105827
1 44240U 19029F   21099.49921094  .05018930  11954-4  19828-2 0  9994
2 44240  52.9833 166.2228 0010694   2.0184 358.0616 16.22873339105096
1 44240U 19029F   21099.62231585  .05403646  11997-4  18908-2 0  9995
2 44240  52.9794 165.5600 0010173 356.9541   3.1435 16.24341295105885
```

The results of the optimal measurement filtration technique to determine the current drag parameter (ballistic factor) are presented in Figure 13.

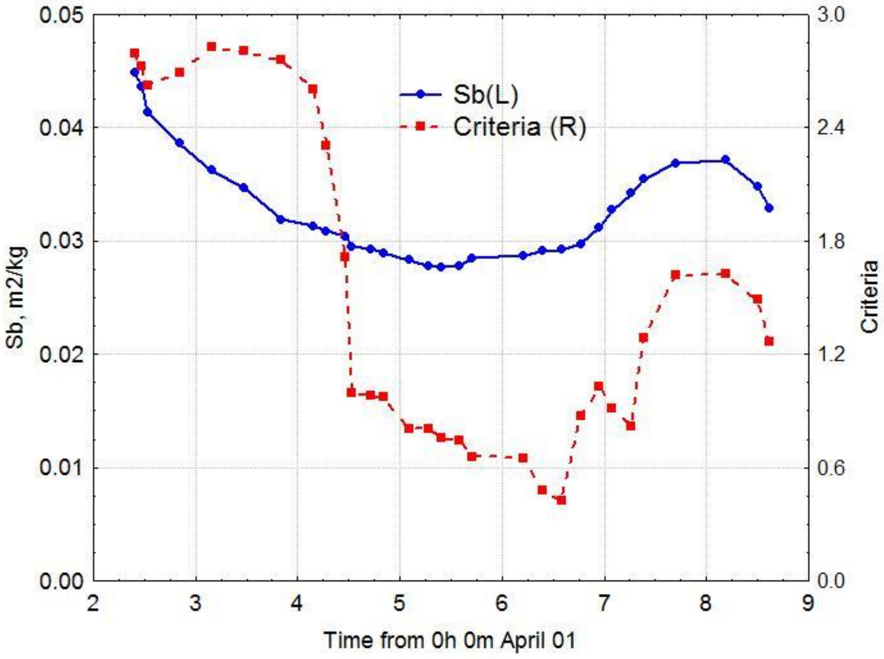

Figure 13. Estimation of ballistic factor (Sb) and minimizing criteria

It is clear from these data that the Sb estimates continue to diminish. They decreased by 3%. This is to be expected, as the geomagnetic storm ended on the night of April 8.

Table 7 provides all estimates of the re-entry time (reaching an altitude of 80 km).

Таблица 7. Determination of **re-entry time**

Time from April 01		Date	hh	mm	ε
Initial	Reentry				
0.219	9.456	April 10	10	56	-0.110
3.47	8.641	April 09	15	22	-0.354
4.841	9.750	April 10	17	59	0.079
5.090	8.820	April 10	19	41	0.097
5.401	9.941	April 10	22	35	0.128
5.588	9.883	April 10	21	11	0.122
5.712	9.799	April 10	19	09	0.107
6.209	9.736	April 10	17	39	0.107
7.264	9.062	April 10	01	29	-0.166
7.388	9.024	April 10	00	35	-0.205
7.697	9.045	April 10	01	05	-0.234
8.191	9.188	April 10	04	31	-0.172
8.499	9.260	April 10	06	14	-0.131
8.622	9.307	April 10	**07**	**21**	-0.077

The data of the last two lines show the increase of the re-entry time by 1 hour 7 minutes (13% of the life time). This is the result of weakening of drag in the atmosphere after the geomagnetic storm (Figure 7). It is important to note here that such a significant change in the satellite drag at the re-entry interval is quite a rare event. The fact is that variations in atmospheric density in geomagnetic storms are highly dependent on altitude. They decrease significantly as the altitude decreases. However, the level of error in the forecast of the re-entry time Statrink-26 satellite was unexpectedly high. Consider the relative errors in determining the re-entry time, which are defined as

$$\varepsilon = error / life\ time\,. \qquad (1)$$

When calculating the relative error (ε) it is necessary to know the real re-entry time of Starlink-26 satellite. Until April 11 author was unable to find information on the Internet about the observation of his re-entry. The next day (April 11), author discovered new data on the site [3]. They are presented in Table 8.

Table 8. NARAD re-tntry data

MSG_EPOCH	INSERT_EPOCH	DECAY_EPOCH	WINDOW	REV	DIRECT	LAT	LONG
2021-04-10 17:17:00	2021-04-10 17:46:14	2021-04-10 **12:27:00**	**2**	10604	descending	-30.3	341.8
2021-04-10 10:30:00	2021-04-10 10:46:14	2021-04-10 12:27:00	24	10604	descending	-30.3	341.8
2021-04-10 07:41:00	2021-04-10 07:56:14	2021-04-10 13:02:00	60	10603	ascending	-12.2	118.6
2021-04-09 21:47:00	2021-04-09 21:56:14	2021-04-10 09:16:00	240	10601	descending	16.7	351.4
2021-04-09 14:10:00	2021-04-09 14:36:14	2021-04-10 08:06:00	240	10601	descending	-40.3	61.9
2021-04-07 16:00:00	2021-04-07 16:06:16	2021-04-10 05:54:00	780	10600	ascending	42.1	278.8
2021-04-06 22:49:00	2021-04-06 22:56:15	2021-04-10 23:18:00	1200	10610	ascending	-39.8	292.5

Red highlighted data inserted after the satellite re-entry. Possible deviations (window) from the estimated decay epoch this case are 2 minute. The second line gives the same estimate of the decay epoch, but with the other window (24 minute). In all cases, the decay epoch estimates are consistent with earlier data. But the question remains: how to explain the coincidence of the decay epoch in the first two lines? The author does not know the answer to this question, but believes that the recent the decay epoch estimates are not reliable enough. This also applies to the declared window (2 minutes). According to all other strings, the window size is at least 15-20% of the life time. Therefore, I have to set this time yourself. I use my latest estimate 07:21 and adjust it slightly to take into account the weakening of drag before the re-entry. Take

$$re\,entry\ time = April\ 10\ 8h\ 38m\,. \qquad (2)$$

The results of the calculation of relative errors (1) are presented in the right column of table 7. The statistical characteristics of these estimates are:

$$M(\varepsilon)=-0.064=6.4\% \quad \sigma(\varepsilon)=0.15=15\%. \qquad (3)$$

Significant difference between the average M(ε) and zero (-6.4%) is explained by the tendency to reduce atmospheric drag at the time interval considered. The resulting value of σ(ε) corresponds to variations in Sb estimates (Figure 13). It is also important to note that the assessment received does not contradict the generally accepted level of accuracy in solving the problem at hand (Table 8).

Figure 14 shows the Earth map and the calculated route of the satellite's movement at re-entry. The red color highlights the possible scattering of the entry point into the dense layers of the atmosphere.

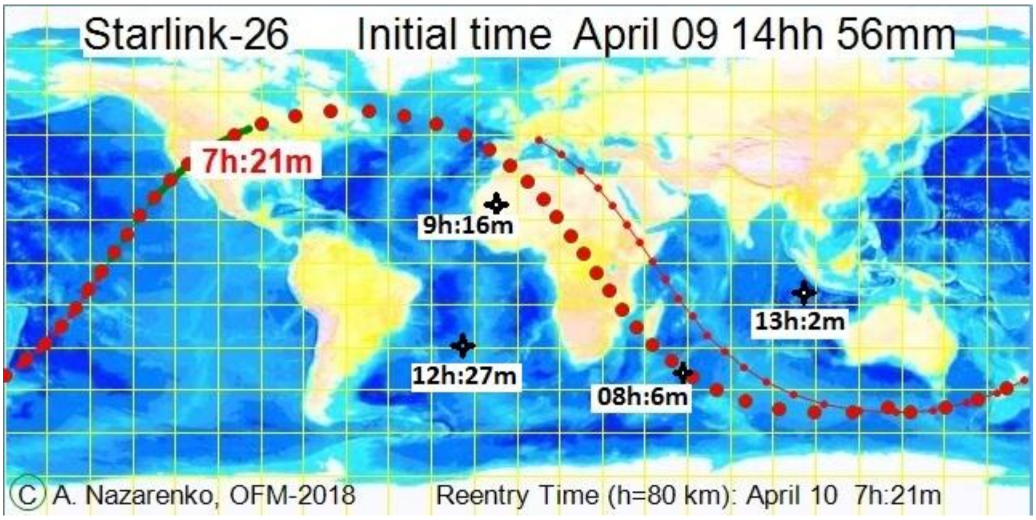

Figure 14. Calculated re-entry route and NORAD data

Our estimate of the re-entry time: 10 April 07h:21m±60m. This result is consistent with NORAD data obtained prior to the satellite's decay (08h:6m), but is not consistent with all subsequent NORAD data. The reasons for such discrepancies are not known to the author.

Conclusion

- Most likely the re-entry time is 10 April 07h:21m±60m.
- This result differs significantly from the site's [3] data.
- The qualitative solution of the problem in question was hampered by significant variations in atmospheric density caused by the geomagnetic storm that occurred on April 7.

References

1. Nazarenko AI. How can we increase the accuracy of determination of spacecraft's lifetime? ActaAstronautica; 2015 Nov 1. 116 :229-36.
2. Назаренко АИ. Задачи стохастической космидинамики. Математиченские методы и алгоритмы решения. М. ЛЕНАНД, 20182-352 с.
3. JSpOC website. Two line element (TLE) data, Satellite decay & reentry data. http://www.space-track.org.
4. Nazarenko AI. Comparison of Various Methods for Orbital Measurements Processing. International Journal of Aeronautical Science & Aerospace Research (IJASAR 2470-4415-06-30), 2019

April 12. 10hh